The Biophysicist

A Laboratory Model for Virus Particle Nanoindentation

William C. Thompson[1], **Angela J. Cattani**[1,2], **Olive Lee**, **Xiang Ma**[1,3], **Irina B. Tsvetkova**[1], **Bogdan Dragnea**[1,*]

[1]Department of Chemistry, Indiana University, Bloomington, IN 47405, USA

ABSTRACT   Self-organization is ubiquitous in biology, with viruses providing an excellent illustration of bioassemblies being much more than the sum of their parts. Following nature's lead, molecular self-assembly has emerged as a new synthetic strategy in the past 3 decades or so. Self-assembly approaches promise to generate complex supramolecular architectures having molecular weights of 0.5 to 100 MDa and collective properties determined by the interplay between structural organization and composition. However, biophysical methods specific to mesoscopic self-assembly, and presentations of the challenges they aim to overcome, remain underrepresented in the educational laboratory curriculum. We present here a simple but effective model for laboratory instruction that introduces students to the world of intermolecular forces and virus assembly, and to a cutting-edge technology, atomic force microscopy nanoindentation, which is able to measure the mechanical properties of single virus shells in vitro. In addition, the model illustrates the important idea that, at nanoscale, phenomena often have an inherent interdisciplinary character.

KEY WORDS   virus shells; mechanics; atomic force microscopy

I. INTRODUCTION

Manifestations of spontaneous self-organization across scales, a hallmark of biologic growth, have captured the imagination of mathematicians, biologists, and physicists alike since the earliest days of molecular biology (1, 2, 3). The structures spontaneously formed by the basic molecular building blocks of living matter, such as lipids, nucleic acids, and proteins, have continued to guide the study of molecular self-assembly driven by noncovalent intermolecular forces and inform a myriad of new technologies in health and energy sciences (2, 4–7).

Viruses are a diverse group of replicating complexes, devoid of their own metabolism, and obligated to their host for essential functions (8). They constitute a unique paradigm in self-assembly because, unlike the majority of synthetic self-assembling complexes, virus particles are often identical at every scale. Viruses have evolved features, such as stoichiometric control, chemical addressability, and reconfigurability, of a sophistication that continues to surpass synthetic self-assembled nanomaterials. These innate characteristics are desirable and potentially critical for many future technologies, such as sustainable energy harvesting (9–11), high latency information storage (12, 13), and nanomedicine (14, 15), in particular, for therapeutic delivery (16) and imaging applications (17–19). Thus, virus organization provides inspiration for innovative, bioenabled self-assembling nanocompartments (20–22), and virus-enabled devices

[2]Current address: Washington University School of Medicine, St. Louis, MO 63110, USA
[3]Current address: Department of Chemistry, Grand View University, Des Moines, IA 50316, USA
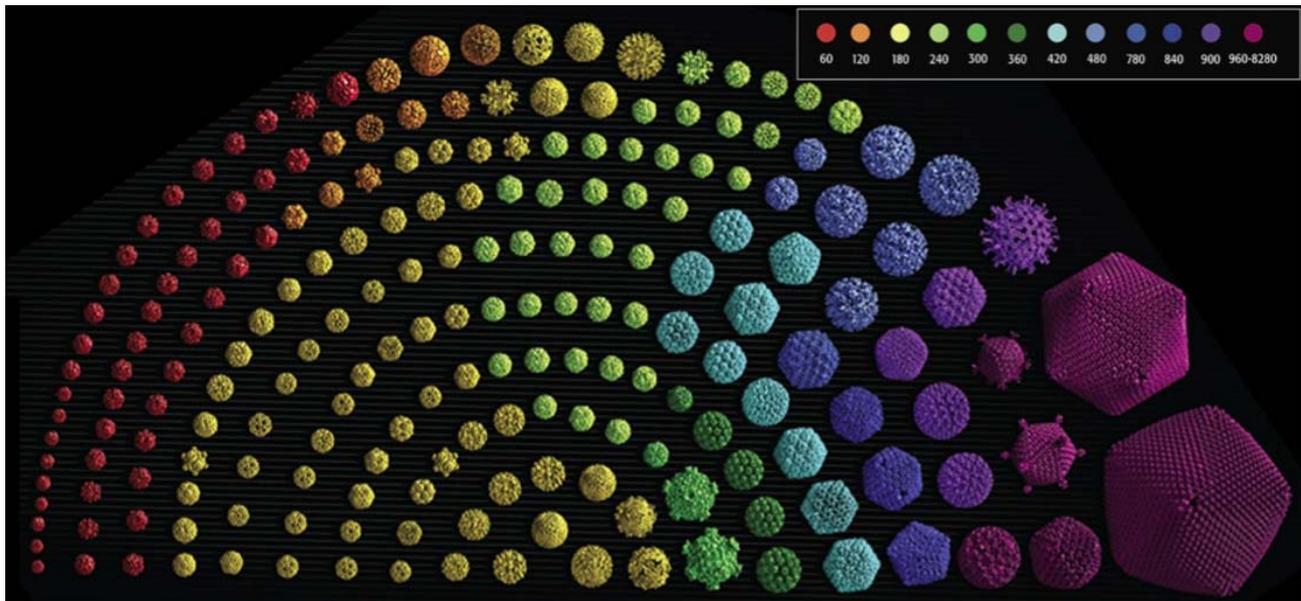
"*" Corresponding author

Fig 1. Viruses having their genomes protected by an icosahedral protein cage span a broad range of sizes. The number of proteins in the shell obeys geometric selection rules captured by several theoretic treatments (29–31). Inset: virus colors describe the number of protein chains in each capsid, adapted from (32).

include photosynthetic systems with efficient energy and electron transfer (23) and higher order complex coupled catalysts (24, 25). In this context, of major interest are virus phenomena and properties concerning assembly, stability, and transformation of viruses that are transferrable by design to an artificial system (26).

At the most basic level, a virus consists of a protein cage (sometimes enveloped in a lipid layer), which encapsulates genomic molecules required for self-perpetuation within a host. Inside the protein cage, known as the capsid, the cargo (mainly genomic ribonucleic acid [RNA] or deoxyribonucleic acid) is often packaged at densities approaching those of a 3-dimensional (3D) crystal (27, 28). Although assembled through much weaker interactions than covalent bonding, and from hundreds to thousands of subunits, the capsids of many viruses from all domains of life show structural similarities. They are often symmetric and remarkably monodisperse (Fig 1; 29–32) because viruses are faced with a challenge: their genomes have to fit into the limited space of a viral capsid, but at the same time, they need to encode all virus proteins. This challenge is solved by using many identical copies of a small protein subunit, which are assembled to form a large capsid.

A host of fundamental questions arise: What role does curvature play in assembly kinetics and capsid thermodynamics? What are the determinants of capsid size? How are dynamics, such as transport across the shell and contact mechanics, influenced by spatial organization? What role do the intrinsic defects encountered in spheric crystallographic lattices play in virus mechanochemistry? Theoretic work is currently leading the way in addressing these questions. However, there is still a strong need for experiments, especially at the scale of a single particle. Answering those questions through theoretic modeling and in vitro experimentation could inform far more than the biophysics of viruses. Thus, focusing on the physical basis of function, such questions are important because they promise to establish a foundation for new design principles in future bioinspired materials. For instance, the biologic advantage of size monodispersity in certain viruses still has to be determined. However, one possible reason is the efficiency of the cell entry process (33, 34). Testing this hypothesis and understanding what ensures the astonishing precision of the assembly process could inform the

design of artificial drug delivery vectors. In teasing out the structure–function relationship it is often required to experiment with and model the collective behavior of molecules that make a virus (21, 35). However, the highly successful methods of structural molecular biology are more apt to interrogate molecular properties in atomic detail than collective phenomena. For instance, looking at the atomic structure of a virus or artificial viruslike particle designed to operate as a delivery vector would provide little (if any) information on the stored mechanical stresses that might influence how the virus interacts with a cell membrane. Thus, the large number of atoms and temporal dynamic range relevant to virus assembly are challenging to theoretic methods with atomic precision (although tremendous progress has been made in the past decade) (35). Most efforts have relied on reduced models that retain those physical aspects, which are hypothesized to be essential. On the basis of these models, computational approaches have generated a wealth of testable hypotheses (36–40). Model validation requires comparison with experiments. The challenge resides in meeting coarse-grained modeling "midway" from the complexities (and uncertainties) of the natural virus environment. In vitro controlled, single-particle mechanochemistry experiments, such as atomic force microscopy (AFM) nanoindentation, amplitude modulation AFM techniques (41, 42), and optical tweezers (43), have revolutionized our understanding of the mechanisms of viral genome packaging and presentation (44–46). However, introducing experimental approaches on the basis of force transduction at the nanoscale has been slow to percolate in the experimental biophysics and chemical physics curriculum. The present article aims at addressing this need.

II. SCIENTIFIC AND PEDAGOGIC BACKGROUND

We present laboratory experiments, amenable to lecture demonstrations or stand-alone undergraduate laboratory projects, which illustrate the basic concepts encountered in icosa-hedral virus assembly and nanoindentation by AFM.

A. Objectives

Most students are familiar with the basic ideas of crystallography and close packing in 2- and 3D flat space from general chemistry courses, which often include an introductory section to the structures and types of solids. In flat space, close packing is ensured by local hexagonal symmetry, which can extend freely throughout the entire space. On a sphere, however, local symmetry cannot propagate throughout. In this case, the growth of a hexagonally packed layer is said to be geometrically frustrated (47). Therefore, any tiling of the surface of a sphere needs to incorporate packing defects, i.e., subunits with a different coordination number than the rest of the lattice. Unlike in the flat space, where defects arise due to kinetics, here students encounter, for the first time, intrinsic defects due to geometric frustration, which must be present in the ground state.

Our objectives are 2-fold: First, we illustrate with a simple experimental model the rules for generating a polyhedral shell assembled by using the same interfacial interactions over and over again, with small necessary deviations due to the presence of intrinsic defects (Fig 2A). Second, we use the same experimental model to study the mechanical properties of polyhedral shells under uniaxial stress, with a scaled-up mechanical setup that mimics virus nanoindentation and is based on the same optical lever idea as the AFM (Fig 2B).

B. Geometric principles of icosahedral cage construction

When coat proteins spontaneously assemble into a sheet, the maximum number of contacts for every subunit is 6. Assuming the free energy drop at assembly is proportional with the number of contacts, Caspar and Klug suggest a geometric model that maximizes the number of contacts in constructing a closed polyhedral shell with quasi-identical subunit–subunit interfaces (29). For isometric particles (i.e., shells that measure equally from a center) the point-
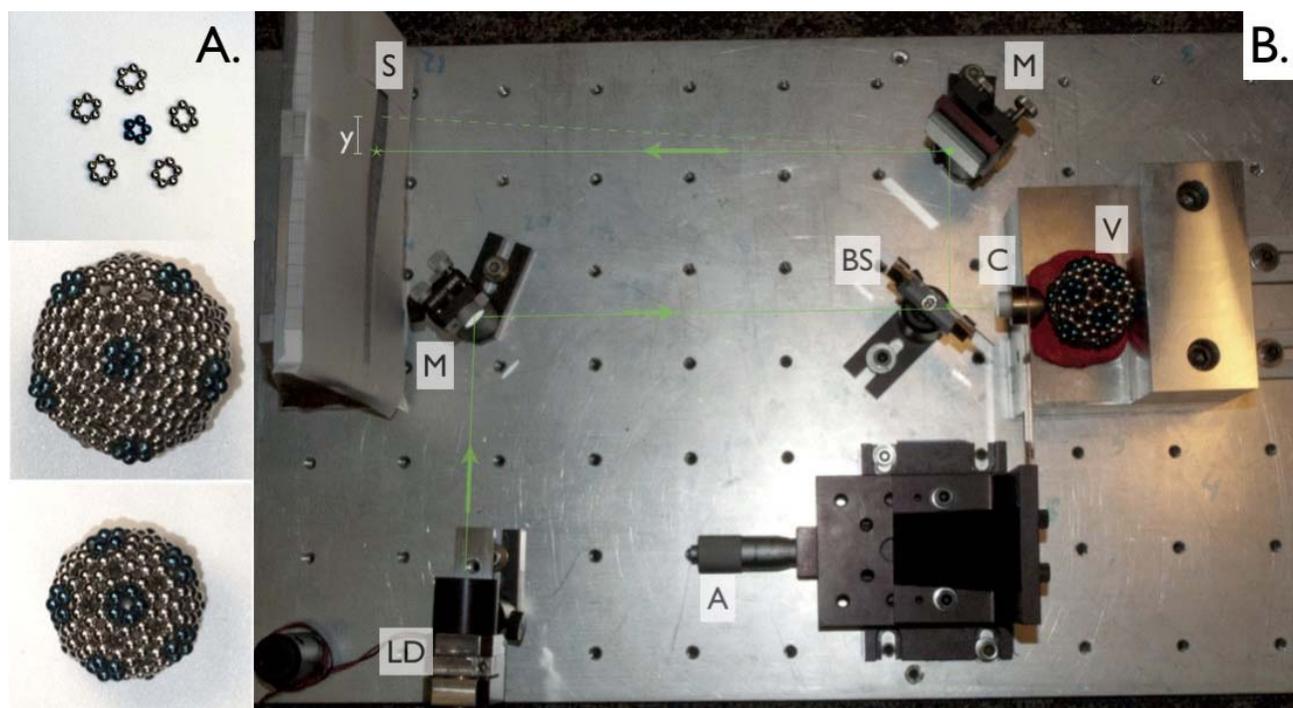
Fig 2. (A) Polyhedral cages formed of pentamers and hexamers constructed from 3-mm NdFeB magnetic beads. (B) Experimental setup for the measurement of force–indentation curves. LD = laser diode, M = mirrors, BS = beam splitter made of microscope glass slide, A = actuator, V = virus cage model, S = screen for display and readout of laser beam deflection, and C = cantilever assembly composed of copper spring blade, mirror, and brass hemisphere as a probe.

group symmetry is cubic (48). Within this group, the regular polyhedron with the largest volume-to-surface ratio is the icosahedron. Indeed, the smallest viruses build icosahedral capsids consisting of 60 copies of a single, small protein. There are 3 protein subunits associated with each equilateral triangular face (see inset in Fig 3), and they are placed at equivalent sites. Such capsids have just enough internal space to hold a genome that encodes a handful of viral proteins.

Longer, more complex genomes of other viruses need larger capsids to accommodate them. Those are constructed from more than 60 subunits of one or more types of proteins. In the Caspar–Klug construction, the capsids are derived from a sheet of hexamers by replacing 12 hexamers by pentamers at appropriate positions in the hexagonal net (49); see Figure 3 (50). One starts by inserting the first pentamer at the origin. The next pentamer position, which defines the length of the icosahedron edge, is given by summing a pair of integer multiples of the lattice unit vectors (h, k). The

third pentameric vertex of the triangular face of the icosahedron is then located through a 60° rotation of the second vertex about the origin. This completes one triangular face. Applying icosahedral symmetry operations to it generates the rest of the icosahedral cage. Subunit arrangements are now only quasisymmetric. However, note that the approach satisfies the physical premise that intersubunit interactions should be nearly preserved across the entire net (Fig 3). The number of proteins in the shell is $T \times 60$, where the integer T is called the triangulation number and obeys the selection rule, $T = h2 + hk + k2$. Thus, there are 12 pentamers and $10(T - 1)$ hexamers in a Caspar–Klug capsid.

The Caspar–Klug construction has been very successful in describing the structures of a large set of viruses. It represents an excellent educational opportunity to show basic geometric and physical principles at work in shaping biologic matter. Thus, in the first part of the project, students will learn to construct
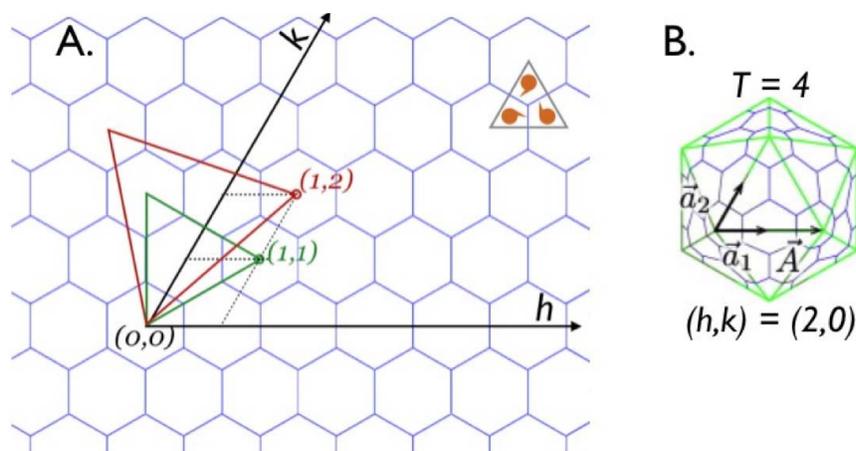
Fig 3. Mapping of a hexagonal net onto an icosahedron according the Caspar–Klug approach (29). (A) The 2 basic triangles from which $T=3$ and $T=7$ cages are constructed. Small triangular inset: 3 protein subunits arranged inside the triangular face of a $T=1$ icosahedron. (B) The final result for a $T=4$ cage ($a_{1,2}$ are the unit vectors for the hexagonal lattice, and A is the vector that indicates where a pentamer replaces a hexamer) (50).

Caspar–Klug cages according their T numbers by using magnetic beads.

C. Mechanics of polyhedral cage deformation

In the second part of the project, students will familiarize themselves with the principles of AFM and virus cage nanoindentation. The magnitude of the Young modulus for the virus coat can be estimated from the spring constant within the framework of the thin elastic shell model (51). Small icosahedral virus Young moduli are comparable in magnitude to those of soft plastics such as Teflon. Such knowledge of the elastic properties of viruses could shed light on the effects of interfacial interactions that viruses experience throughout their life cycle.

AFM imaging is now firmly established as a biophysical tool (52), and there are numerous references that will provide a good introduction to it; see, for example (53). Figure 4 provides a cartoon outlining the main principle features of topographic AFM imaging. Our focus here is to introduce AFM as a nano-indentation tool, which can inform the elastic properties of viruses within the framework of the continuum elastic theory of shells and beyond.

A diagram of the AFM indentation experiment is presented in Figure 5. In a typical AFM nanoindentation experiment, a spread of virus particles adsorbed on a solid support is first imaged. Then, the AFM probe is placed on top of a virus particle, and the probe is pressed against the virus particle through a series of small, calibrated steps in a direction normal to the substrate surface. At each step, the extension of the pushing actuator, Δz, and the deflection of the laser probe, Δy, resulting from it, are recorded. Then, we have (Fig 5)

$$\Delta z = \Delta x + \Delta u \qquad (1)$$

where x is the indentation of the sample and u is the linear vertical displacement of the tip, relative to the straight cantilever position purely due to cantilever bending, as it presses on the sample. Assuming the cantilever and the virus act as 2 springs in series compressed by an external force, at each actuator step Δz, the changes Δu and Δx are related through the elastic constants of the virus (kv) and the cantilever (kc):

$$kv \cdot \Delta x = kc \cdot \Delta u \qquad (2)$$

Cantilever deflection is measured by recording the shift, y, in the laser spot location on a distant, position-sensitive detector. The optical lever gain, G, can be found by pushing the probe into a surface of high stiffness. G is simply $\Delta y/\Delta z$ in that case. With the G factor known, we have
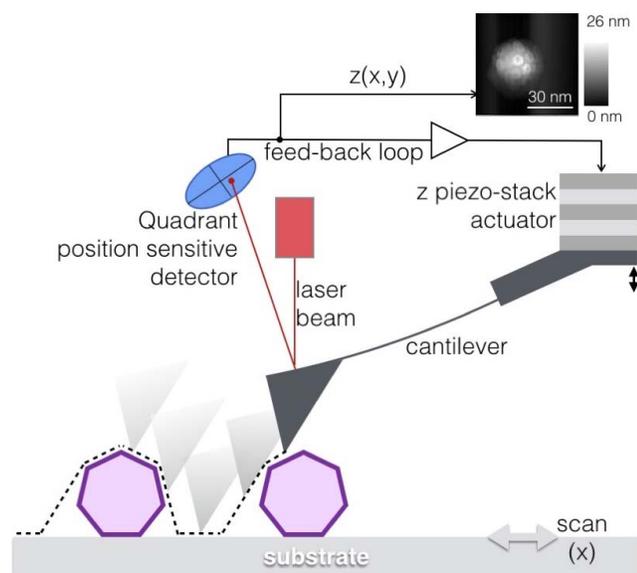
Fig 4. Schematic of AFM imaging of virus particles. The force (and thus the distance) between the AFM probe and the sample is kept constant, while raster scanning the sample at a distance of ~ 1 nm via a feedback loop driving a fast piezo actuator (z piezo stack). Positional adjustments of the vertical piezo are then displayed as a topographic map (z versus x and y).

Fig 5. Diagram of the AFM indentation experiment. L = laser, A = piezo-actuator, C = cantilever with hemispheric probe and mirror. Distances: z = actuator displacement, x = shell indentation, u = linear cantilever deflection, y = optical lever deflection.

$$\Delta y = G \cdot \Delta u \qquad (3)$$

To determine the compression force from deflection, the cantilever constant, kc, is required. It is customarily obtained by fitting the thermal noise oscillation spectrum with a harmonic oscillator model at thermal equilibrium (54, 55).

Raw experimental data is usually represented as deflection Δy (or force), as a function of actuator displacement Δz. Assuming the virus behaves as a Hookean material, from the measurement of Δy and Δz and using Eqs. 1–3, one can obtain an effective elastic constant for the virus particle, kv.

In practice, the simplest way to extract the Young modulus, E, for the capsid material from kv is to approximate the capsid with a thin spheric shell (51). However, this approach is expected to overestimate E because it does not account for the site-dependent deformation of capsid protein subunits themselves, which will generally produce a state of prestress within the icosahedral shell (50, 56, 57). Nevertheless, kv is considered an adequate practical descriptor of the mechanical state of a virus and was shown to reflect
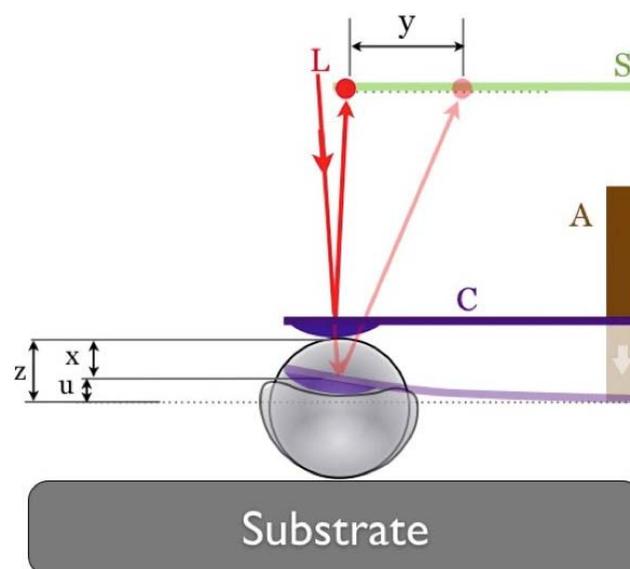
changes occurring as result of virus life stages or environmental cues (58–60).

III. MATERIALS AND METHODS

A. Construction of Caspar–Klug polyhedral cages from discrete subunits

For a practical introduction to the Caspar–Klug construction, cages made of 3-mm magnetic beads as subunits make a useful representation. We start the shell assembly from a set that includes 2 oligomeric subassemblies: ringlike pentamers and hexamers, which we call capsomers (Fig 2A). Assuming the ringlike capsomers are in their minimum energy state, to attract, 2 capsomers should have the magnetic dipoles running in the same direction around the ring (i.e., both clockwise or both anticlockwise). Thus, if 2 capsomers repel, to make them stick, 1 must be flipped. Starting from a pentamer, we build concentric rings of capsomers around it according the Caspar–Klug scheme (see Supplemental Video S1 in the Supplemental Material for a $T = 3$ example).

B. Optomechanical setup

The entire optomechanical setup is shown in Figure 2B. The most expensive part is the laser pointer. The cantilever can be inexpensively machined out of a strip of metal sheet, and inexpensive mirrors and kinematic mounts will give satisfactory results. In our setup, we used a $150 \times 30 \times 1$-mm strip of copper or brass for the cantilever shaft. It can be shown that, for best signal to noise, the AFM cantilever elastic constant has to be similar with that of the cage. However, as that has to do with the amplitude of thermal fluctuations, it is not directly relevant to the scaled-up mechanical system here.

The cantilever was clamped in a mount over 40 mm of its length. For the probe, we have used an 8-mm-radius hemisphere, which mimicked the AFM tip. On the other side of the probe, on the cantilever shaft, we glued a 12-mm mirror. The laser beam was aligned at normal incidence onto this mirror. When the probe met a surface, the beam would start to deflect. The actuator used for probe displacement was a differential micrometer screw with a Vernier scale, with a precision of 0.05 mm. The laser spot position as a function of actuator displacement was read onto a millimeter graph paper screen. The optical lever length measured from the cantilever mirror to the screen was about 600 mm.

We have not calibrated the cantilever, as the experiments we have carried out solely involved comparisons of cage orientations, with respect to the compression direction and between spheric thin shells and icosahedral shells. If required, to calibrate the cantilever one can measure the mass of small metal weights by using an electronic scale and the respective deflection, resulting from placing each weight onto the cantilever.

C. Sample preparation for AFM indentation of brome mosaic virus particles

In the next section, we present a comparison of the force–displacement curves acquired from a $T = 3$ magnetic bead cage and from brome mosaic virus (BMV) particles adsorbed on a highly oriented pyrolytic graphite surface in aqueous solution. The BMV has a $T = 3$ capsid, composed of 180 identical coat proteins, and is a very well-studied model for small, nonenveloped, single-stranded RNA viruses (61). Sample preparation and AFM indentation protocols for BMV have been described elsewhere (46), and there is a detailed description of the generic features of the experiment in (62).

IV. RESULTS AND DISCUSSION

A. Prestress

When the model is assembled under its constitutive magnetic interactions, it looks fairly spheric. When we add to the spheric shape, the observation that 2 spheric beads make contact at a point and, therefore, the contact area between subunits is very small, it is tempting to expect that the mechanical behavior of the cage under compression should be similar to that of a thin elastic spheric shell. In these conditions, it should be irrelevant whether we push along a 3-fold versus a 5-fold symmetry axis (Fig 6). The mechanical response as embodied in the deflection versus displacement curve and within the thin spheric shell approximation should be the same. Experiments done on a $T = 3$ cage on 2 orientations (compression along a 5-fold and along a 3-fold) are presented in Figure 7, as deflection (same as force) versus actuator displacement, together with deflection–displacement data taken on the substrate (no cage). Compression forces in this case were low enough to observe partial reversibility.

The elastic constant of the cages was evaluated from the initial slope of the deflection–displacement curve. Clearly, compressing along the 5-fold axis yields a significantly stiffer response from the particle than if we compress along the 3-fold axis, because the magnetic cage is prestressed with the pentameric defects being under high stress in this case. For in-depth discussions of this many-body effect see (36, 50, 63).

The difference in stiffness between a 5- and a 3-fold axis depends on the radius and the ratio between the bending modulus and the stretch-

Fig 6. Three orientations of the $T = 3$ cage. From left to right: 2-, 3-, and 5-fold symmetry axes, normal to the viewer.

ing modulus of the shell material (64). Thus, orientation effects originating in prestress are expected and have been observed experimentally on viruses (65). One of the practical implications of the effect could be a preferential orientation upon contact with the cell surface. For instance, it was found that BMV orients preferentially with a 3-fold axis down on a rigid surface, whether it is a hydrophobic or hydrophilic surface (66).

B. Compression beyond the linear regime

In the previous section, we have limited our analysis to small indentations and quasielastic response. It is interesting to compare the behavior of the macroscopic model with that of a virus over a broader range of strain. Figure 8 shows a comparison of force–compression curves obtained from the magnetic model and by AFM from BMV for 2 orientations.

There is surprising qualitative similarity between the force–compression curves of the magnetic model and the virus: we observe a similar sequence of buckling events (drops in force and deflection as the strain increases). We also observe that there is partial recovery in both the virus and the magnetic cage when compressing on the 3-fold axis, but very little, if any, occurs when compressing on the 2-fold axis. On the model, it is easy to observe the structural changes that accompany buckling. They are, in general, involving patches (spheric
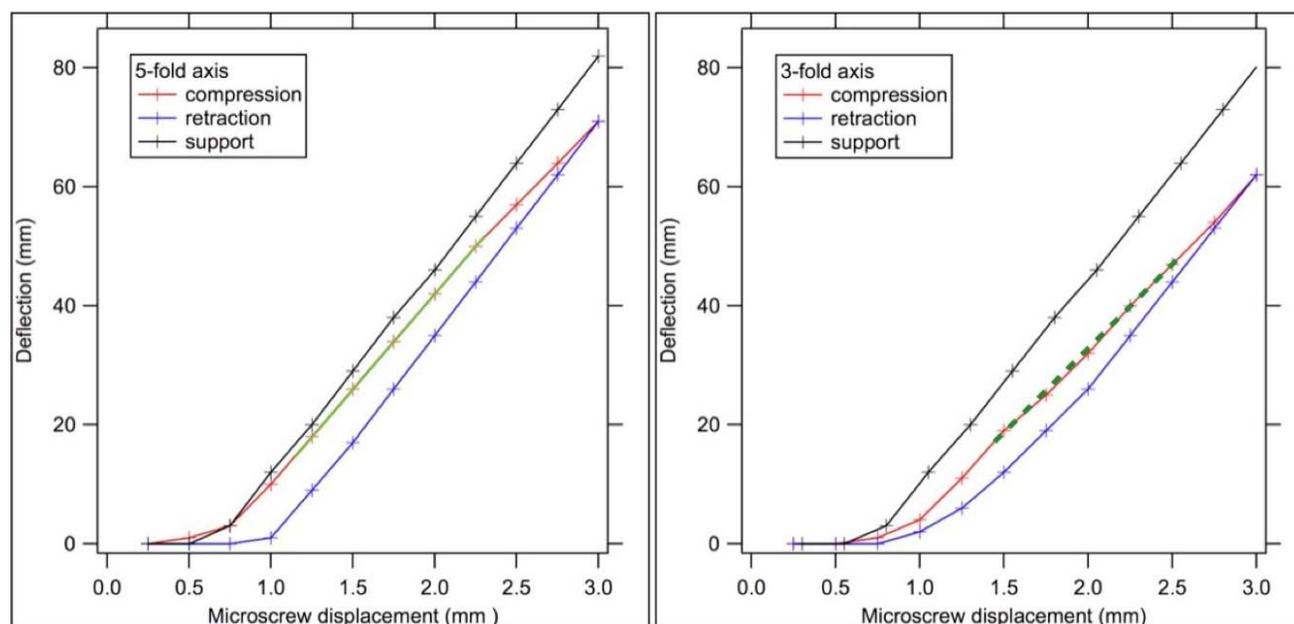

Fig 7. Indentation of the magnetic cage model with a small force, at 2 different cage orientations: 5-fold (left) and 3-fold (right). The black curve is obtained by compressing the substrate directly. The green line is a linear fit to the compression curve for the 5-fold orientation, and the dashed green line is a linear fit for the 3-fold orientation. The slope of the linear fit gives the sample stiffness. The 5-fold orientation corresponds to a steeper slope, and, thus, the highest stiffness.
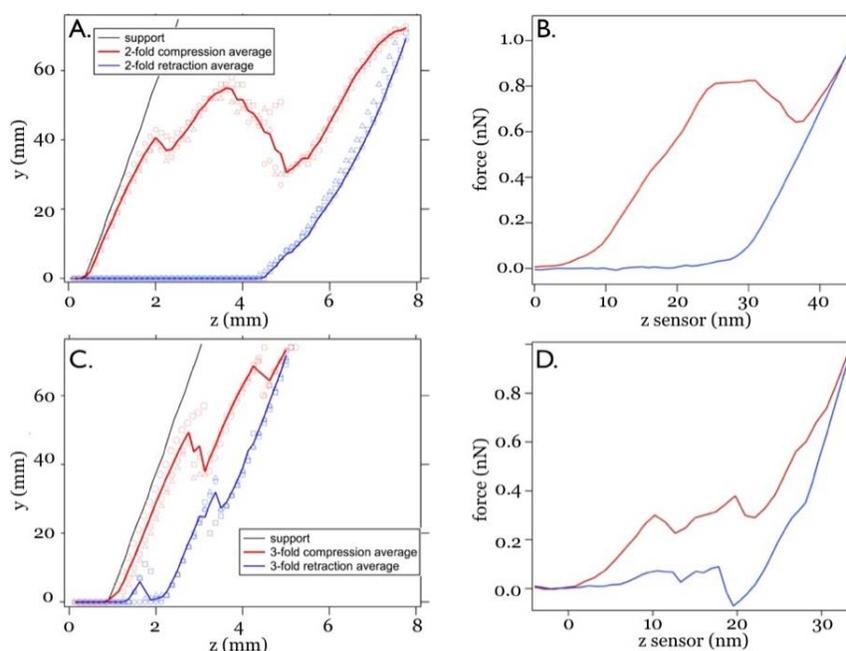
Fig 8. (A) Indentation of the magnetic cage model to about 30% of its initial height, along a 2-fold axis. (B) Indentation of BMV along a 2-fold axis. (C) Indentation of the magnetic model along a 3-fold axis. (D) Indentation of the virus along a 3-fold axis.

sectors) moving as a whole, which are isometric with respect to the contact area of the probe.

The similarities between the stress–strain relationship in magnetic bead cages and virus shells suggest that common mechanical principles are involved in large-scale deformations. However, when discussing these similarities, students should be made aware of the important differences that separate the macroscopic model from the microscopic virus system. In the latter, entropy, reversibility, and contributions of the nucleic acid to the free energy of deformation (see, e.g., 67, 68) play major roles that are not recapitulated by the model.

We gave 2 examples of types of projects and discussions that can be carried out. Many other interesting experiments could be envisioned. For instance, in terms of structure and symmetry, students could be provided an assembled magnetic capsule and be asked to determine what T number it is and how many different subunit–subunit interfaces they could identify. In terms of mechanics, they could be asked to investigate the role of shear. In the magnetic bead capsule, the beads can move past each other during deformation, but how would the force–compression curve be different if we did

not allow for it to occur, for example, if we replaced the cage by a 3D-printed polymer replica? We could also ask: What if there are vacancy defects, such as those observed in immature human immunodeficiency virus shells? How would the stiffness and overall force–compression curve change? Also, finite size effects, which have no counterpart in bulk materials, are expected to play a role in the mechanical response; these could be easily explored as well. In this regard, a recent article found that even at small stresses, well below the yielding point and generally thought to induce a Hookean response, strain continues to develop in time via sparse, randomly distributed, relatively rapid plastic events (69). Such events are believed to be initiated as dislocations between a pentameric and a hexameric unit and propagate as cracks as the mechanical loading increases. Could these be recapitulated by the magnetic capsule model? Would such intermittency of deformation be present in capsules in which all sites are strictly identical from the point of view of binding strength and geometry (for example, in magnetic bead cylinders)? These are only a few suggestions of further questions and explorations; the model is suitable for an even broader scope

of discussion. An example in this sense is the virology blog kept by Racaniello (70).

V. CONCLUSION

In conclusion, we have presented a magnetic bead cage demonstration to illustrate experimentally how to construct icosahedral virus cage models and how to probe virus biomechanics. Using a simple instrument, which can be constructed by high school and undergraduate students, we have quantified the Hookean response of viromimetic magnetic bead cages at low mechanical stress and observed orientation-dependent buckling transitions at high mechanical stress. We have also observed the occurrence of prestress, which, similar to virus cages, can be related to inherent geometric frustration.

SUPPLEMENTAL MATERIAL

A video of the step-by-step magnetic bead $T = 3$ cage construction described in Materials and Methods is available at: https://doi.org/10.35459/tbp.2019.000106.S1.

AUTHOR CONTRIBUTIONS

WCT constructed the apparatus and performed experiments. AJC, OL, and XM performed research and analyzed data. BD wrote the manuscript, IBT created the visual aids, and BD designed the research.

REFERENCES

1. Thompson, D. W. 1942. On Growth and Form. Courier Dover Publications, Mineola, NY.
2. Bernal, J. D. 1957. The scale of structural units in biopoesis. In The Origin of Life on the Earth. A. I. Oparin, A. E. Braunshteĭn, A. G. Pasynskiĭ, and T. E. Pavlovskaya, editors. Pergamon, Oxford, United Kingdom, pp. 385–399.
3. Mathai, A. M., and T. A. Davis. 1974. Constructing the sunflower head. *Math Biosci* 20(1–2):117–133.
4. Crane, H. R. 1950. Principles and problems of biological growth. *Sci Mon* 70(6):376–389.
5. Asakura, S., and F. Oosawa. 1954. On interaction between two bodies immersed in a solution of macromolecules. *J Chem Phys* 22(7):1255–1256.
6. Seeman, N. C., and A. M. Belcher. 2002. Emulating biology: building nanostructures from the bottom up. *Proc Natl Acad Sci U S A* 99(Suppl 2):6451–6455.
7. Israelachvili, J., and I. Ladyzhinski. 2005. The physico-chemical basis of self-assembling structures. In Forces, Growth and Form in Soft Condensed Matter: At the Interface between Physics and Biology. NATO Science Series II: Mathematics, Physics and Chemistry. A. T. Skjeltorp and A. V. Belusjkin, editors. Springer Nature, Berlin, pp. 1–28.
8. Flint, S. J., L. W. Enquist, V. R. Racaniello, and A. M. Skalka. 2009. Principles of Virology, vol. 1. John Wiley and Sons, Hoboken, NJ.
9. Serrano, E., G. Rus, and J. García-Martínez. 2009. Nanotechnology for sustainable energy. *Renew Sustain Energy Rev* 13(2009):2373–2384.
10. Lee, Y. J., H. Yi, W.-J. Kim, K. Kang, D. S. Yun, M. S. Strano, G. Cedar, and A. M. Belcher. 2009. Fabricating genetically engineered high-power lithium-ion batteries using multiple virus genes. *Science* 324(5930):1051–1055.
11. Oh, D., J. Qi, B. Han, G. Zhang, T. J. Carney, J. Ohmura, Y. Zhang, Y. Shao-Horn, and A. M. Belcher. 2014. M13 virus-directed synthesis of nanostructured metal oxides for lithium-oxygen batteries. *Nano Lett* 14(8):4837–4835.
12. Church, G. M., Y. Gao, and S. Kosuri. 2012. Next-generation digital information storage in DNA. *Science* 337(6102):1628.
13. Geller, T. 2014. The forever disc. *Commun ACM* 57(5):24–26.
14. Yildiz, I., S. Shukla, and N. F. Steinmetz. 2011. Applications of viral nanoparticles in medicine. *Curr Opin Biotechnol* 22(6):901–908.
15. Schwarz, B., and T. Douglas. 2015. Development of virus-like particles for diagnostic and prophylactic biomedical applications. *Wiley Interdiscip Rev Nanomed Nanobiotechnol* 7(5):722–735.
16. Judd, J., M. L. Ho, A. Tiwari, E. J. Gomez, C. Dempsey, K. Van Vliet, O. A. Igoshin, J. J. Silberg, M. Agbandje-McKenna, and J. Suh. 2014. Tunable protease-activatable virus nanonodes. *ACS Nano* 8(5):4740–4746.
17. Huang, X., B. D. Stein, H. Cheng, A. Malyutin, I. B. Tsvetkova, D. V. Baxter, N. B. Remmes, J. Verchot, C. Kao, L. M. Bronstein, and B. Dragnea. 2011. Magnetic virus-like nanoparticles in *N. benthamiana* plants: a new paradigm for environmental and agronomic biotechnological research. *ACS Nano* 5(5):4037–4045.
18. Usselman, R. J., S. Qazi, P. Aggarwal, S. S. Eaton, G. R. Eaton, S. Russek, and T. Douglas. 2015. Gadolinium-loaded viral capsids as magnetic resonance imaging contrast agents. *Appl Magn Reson* 46(3):349–355.
19. Jung, B., A. L. N. Rao, and B. Anvari. 2011. Optical nano-constructs composed of genome-depleted brome mosaic virus doped with a near infrared chromophore for potential biomedical applications. *ACS Nano* 5(2):1243–1252.
20. Pandey, S., M. Ewing, A. Kunas, N. Nguyen, D. H. Gracias, and G. Menon. 2011. Algorithmic design of self-folding polyhedral. *Proc Natl Acad Sci U S A* 108(50):19885–19890.
21. Aumiller, W. M., M. Uchida, and T. Douglas. 2018. Protein cage assembly across multiple length scales. *Chem Soc Rev* 47(1):3433–3469.
22. Edwardson, T. G. W., and D. Hilvert. 2019. Virus-inspired function in engineered protein cages. *J Am Chem Soc* 141(24):9432–9443.
23. Ma, Y.-Z., R. A. Miller, G. R. Fleming, and M. B. Francis. 2008. Energy transfer dynamics in light-harvesting assemblies templated by the tobacco mosaic virus coat protein. *J Phys Chem B* 112(22):6887–6892.
24. Casey, J. P., R. J. Barbero, N. Heldman, and A. M. Belcher. 2014. Versatile *de novo* enzyme activity in capsid proteins from an engineered M13 bacteriophage library. *J Am Chem Soc* 136(47):16508–16514.
25. Liu, A., M. V. de Ruiter, S. J. Maassen, and J. J. L. M. Cornelissen. 2018. Nanoreactors via encapsulation of catalytic gold nanoparticles within cowpea chlorotic mottle virus protein cages. In Protein Scaffolds: Design, Synthesis, and Applications. A. K. Udit, editor. Humana Press, Totowa, NJ, pp. 1–9.
26. Padilla, J. E., C. Colovos, and T. O. Yeates. 2001. Nanohedra: using symmetry to design self assembling protein cages, layers, crystals, and filaments. *Proc Natl Acad Sci U S A* 98(5):2217–2221.
27. Bruinsma, R. F. 2006. Physics of RNA and viral assembly. *Eur Phys J E* 19(3):303–310.
28. Gelbart, W. M., and C. M. Knobler. 2009. Virology: pressurized viruses. *Science* 323(5922):1682–1683.
29. Caspar, D. L. D., and A. Klug. 1962. Physical principles in construction of regular viruses. *Cold Spring Harb Symp Quant Biol* 27:1–24.
30. Lorman, V. L., and S. B. Rochal. 2007. Density-wave theory of the capsid structure of small icosahedral viruses. *Phys Rev Lett* 98(18):185502.
31. Twarock, R. 2006. Mathematical virology: a novel approach to the structure and assembly of viruses. *Philos Trans R Soc A* 364(1849):3357–3373.
32. Goodsell, D. 2019. RCSB PDB-101: educational portal of PDB: quasisymmetry in icosahedral viruses. Accessed 9 April 2020. http://pdb101.rcsb.org/motm/200.
33. Agudo-Canalejo, J., and R. Lipowsky. 2015. Critical particle sizes for the engulfment of nanoparticles by membranes and vesicles with bilayer asymmetry. *ACS Nano* 9(4):3704–3720.

34. Frey, F., F. Ziebert, and U. S. Schwarz. 2019. Stochastic dynamics of nanoparticle and virus uptake. *Phys Rev Lett* 122(8):088102.

35. Tarasova, E., and D. Nerukh. 2018. All-atom molecular dynamics simulations of whole viruses. *J Phys Chem Lett* 9(19):5805–5809.

36. Zandi, R., and D. Reguera. 2005. Mechanical properties of viral capsids. *Phys Rev E* 72(2):021917.

37. Siber, A., and R. Podgornik. 2009. Stability of elastic icosadeltahedral shells under uniform external pressure: application to viruses under osmotic pressure. *Phys Rev E Stat Nonlinear Soft Matter Phys* 79(1):011919.

38. Nguyen, H. D., V. S. Reddy, C. L. Brooks III, and C. L. Brooks. 2009. Invariant polymorphism in virus capsid assembly. *J Am Chem Soc* 131(7):2606–2614.

39. Hagan, M. F., and R. Zandi. 2016. Recent advances in coarse-grained modeling of virus assembly. *Curr Opin Virol* 18:36–43.

40. Li, S., P. Roy, A. Travesset, and R. Zandi. 2018. Why large icosahedral viruses need scaffolding proteins. *Proc Natl Acad Sci U S A* 115(43):10971–10976.

41. Roos, W. H., R. Bruinsma, and G. J. L. Wuite. 2010. Physical virology. *Nat Phys* 6:733–743.

42. Efremov, Y. M., A. X. Cartagena-Rivera, A. I. M. Athamneh, D. M. Suter, and A. Raman. 2018. Mapping heterogeneity of cellular mechanics by multi-harmonic atomic force microscopy. *Nat Protoc* 13(10):2200–2216.

43. Bustamante, C., J. C. Macosko, and G. J. L. Wuite. 2000. Grabbing the cat by the tail: manipulating molecules one by one. *Nat Rev Mol Cell Biol* 1(2):130–136.

44. Gelbart, W. M., and C. M. Knobler. 2008. The physics of phages. *Phys Phages* 61(1):42–47.

45. Mateu, M. G. 2012. Mechanical properties of viruses analyzed by atomic force microscopy: a virological perspective. *Virus Res* 168(1–2):1–22.

46. Vaughan, R., B. Tragesser, P. Ni, X. Ma, B. Dragnea, and C. C. Kao. 2014. The tripartite virions of the brome mosaic virus have distinct physical properties that affect the timing of the infection process. *J Virol* 88(11):6483–6491.

47. Sadoc, J.-F., and R. Mosseri. 2006. Geometrical Frustration, vol. 23. Cambridge University Press, Cambridge.

48. Crick, F. H. C., and J. D. Watson. 1956. Structure of small viruses. *Nature* 177:473–475.

49. Johnson, J. E., and J. A. Speir. 1997. Quasi-equivalent viruses: a paradigm for protein assemblies. *J Mol Biol* 269(5):665–675.

50. Perotti, L. E., A. Aggarwal, J. Rudnick, R. Bruinsma, and W. S. Klug. 2015. Elasticity theory of the maturation of viral capsids. *J Mech Phys Solids* 77:86–108.

51. Michel, J. P., I. L. Ivanovska, M. M. Gibbons, W. S. Klug, C. M. Knobler, G. J. L. Wuite, and C. F. Schmidt. 2006. Nanoindentation studies of full and empty viral capsids and the effects of capsid protein mutations on elasticity and strength. *Proc Natl Acad Sci U S A* 103(16):6184–6189.

52. Santos, N. C., and M. A. Castanho. 2004. An overview of the biophysical applications of atomic force microscopy. *Biophys Chem* 107(2):133–149.

53. de Pablo, P. J., and M. Carrión-Vásquez. 2014. Imaging biological samples with atomic force microscopy. *Cold Spring Harb Protoc* 2014(2):167–177.

54. Hutter, J. L., and J. Bechhoefer. 1993. Calibration of atomic force microscope tips. *Rev Sci Instrum* 64:1868–1873.

55. Proksch, R., T. E. Schäffer, J. P. Cleveland, R. C. Callahan, and M. B. Viani. 2004. Finite optical spot size and position corrections in thermal spring constant calibration. *Nanotechnology* 15(9):1344–1350.

56. Baclayon, M., G. K. Shoemaker, C. Uetrecht, S. E. Crawford, M. K. Estes, B. V. V. Prasad, A. J. R. Heck, G. J. L. Wuite, and W. H. Roos. 2011. Prestress strengthens the shell of Norwalk virus nanoparticles. *Nano Lett* 11(11):4865–4869.

57. Klug, W. S., W. H. Roos, and G. J. L. Wuite. 2012. Unlocking internal prestress from protein nanoshells. *Phys Rev Lett* 109(16):168104.

58. Pang, H.-B., L. Hevroni, N. Kol, D. M. Eckert, M. Tsvitov, M. S. Kay, and I. Rousso. 2013. Virion stiffness regulates immature HIV-1 entry. *Retrovirology* 10:4.

59. Castellanos, M., R. Pérez, C. Carrasco, M. Hernando-Pérez, J. Gómez-Herrero, P. J. de Pablo, and M. G. Mateu. 2012. Mechanical elasticity as a physical signature of conformational dynamics in a virus particle. *Proc Natl Acad Sci U S A* 109(30):12028–12033.

60. Snijder, J., V. S. Reddy, E. R. May, W. H. Roos, G. R. Nemerow, and G. J. L. Wuite. 2013. Integrin and defensin modulate the mechanical properties of adenovirus. *J Virol* 87(5):2756–2766.

61. Kao, C. C., and K. Sivakumaran. 2000. Brome mosaic virus, good for an RNA virologist's basic needs. *Mol Plant Pathol* 1(2):91–97.

62. Roos, W. H. 2011. How to perform a nanoindentation experiment on a virus. *Methods Mol Biol* 783:251–264.

63. Bowick, M., A. Cacciuto, D. R. Nelson, and A. Travesset. 2002. Crystalline order on a sphere and the generalized Thomson problem. *Phys Rev Lett* 89(18):185502.

64. Lidmar, J., L. Mirny, and D. R. Nelson. 2003. Virus shapes and buckling transitions in spherical shells. *Phys Rev E* 68(4710):51910.

65. Roos, W. H., M. M. Gibbons, A. Arkhipov, C. Uetrecht, N. R. Watts, P. T. Wingfield, A. C. Steven, A. J. R. Heck, K. Schulten, W. S. Klug, and G. J. L. Wuite. 2010. Squeezing protein shells: how continuum elastic models, molecular dynamics simulations, and experiments coalesce at the nanoscale. *Biophys J* 99(4):1175–1181.

66. Zeng, C., M. Hernando-Pérez, B. Dragnea, X. Ma, P. van der Schoot, and R. Zandi. 2017. Contact mechanics of a small icosahedral virus. *Phys Rev Lett* 119(3):038102.

67. Hernando-Perez, M., R. Miranda, M. Aznar, J. L. Carrascosa, I. A. T. Schaap, D. Reguera, and P. J. de Pablo. 2012. Direct measurement of phage phi29 stiffness provides evidence of internal pressure. *Small* 8(15):2366–2370.

68. Hernando-Perez, M., A. X. Cartagena-Rivera, A. L. Bozic, P. J. P. Carrillo, C. S. Martin, M. G. Mateu, A. Raman, R. Podgornik, and P J. de Pablo. 2015. Quantitative nanoscale electrostatics of viruses. *Nanoscale* 7(41):17289–17298.

69. Hernando-Pérez, M., C. Zeng, M. C. Miguel, and B. Dragnea. 2019. Intermittency of deformation and the elastic limit of an icosahedral virus under compression. *ACS Nano* 2019(13):7842–7849.

70. Racaniello, V. 2018. Virology Blog. Accessed 4 April 2020. http://www.virology.ws/2018/03/13/virus-watch-buckyball-viruses/.